Evaluating the Electro-Magnetic Effects of Electrical Short-Circuits in a Nb-Ti Accelerator Magnet

V. Reynaud, S. Farinon, M. Janitschke, E. Ravaioli, A.P. Verweij, G. Willering, and U. van Rienen

***Abstract*—Electrical short-circuits in the coil winding pack of a superconducting magnet can severely impact the magnet's performance and safety during operation. Hence, finding ways to detect and assess these non-conformities is essential. Measurements of the complex impedance as a function of the frequency are a promising method to investigate such non-conformities more closely. The complex impedance of one HL-LHC recombination dipole magnet was recently measured at the CERN magnet test facility. Moreover, to mimic an inter-turn short in the coils, resistances at warm were connected externally to the voltage taps and the complex impedance of the magnet was measured. The acquired measurements are used to validate a developed lumped-element network model, reproducing the electromagnetic behaviour of the HL-LHC recombination dipole magnet in the frequency domain. The simulation results are compared to the measurements without artificial short circuits and are in good agreement up to a frequency of 10 kHz. The simulated effects of short circuits across a few turns in the frequency domain are compared to the measurements performed on the magnet. Since good agreement between measurements and simulations was obtained, these models can be used to predict the electromagnetic effects of any inter-turn short in the HL-LHC recombination dipole magnet or similar types of accelerator magnets.**

***Index Terms*—AC-loss, accelerator magnet, fault diagnostics, frequency-domain, impedance measurements, superconducting coil.**

I. Introduction

SUPERCONDUCTING magnets are critical components in particle accelerators like the Large Hadron Collider (LHC) at CERN. They generate strong magnetic fields that maintain the circular trajectory of charged particles, allowing the collider to achieve high energies. Ensuring the reliability of these magnets is essential for reaching high availability of the collider. However, the performance of the magnets can be compromised by faults such as inter-turn shorts, which may occur during operation due to heat and mechanical stress, and can cause severe damage during quenching or fast ramping.

A promising method for diagnosing these faults involves measurements of the complex impedance as a function of frequency. These measurements provide valuable insights into the magnet's electromagnetic behavior, potentially detecting precursors of anomalies like inter-turn shorts. Similar methods have already been used [1] to detect short-circuits in non-planar coils in fusion stellarators [2][3], in CICC model coils [4], and to monitor and control the resin impregnation process in Nb_3Sn coils [5]. Lumped-element network modeling has been shown to be an efficient approach for simulating the behavior of superconducting magnet circuits in the frequency domain [6], [7], potentially helping to detect anomalies and ensure electrical reliability.

This study aims to validate a two-dimensional network model of the HL-LHC Main Bending Recombination Dipole (MBRD) using a recently developed lumped-element physics-driven model [6]. This model accurately simulates the complex impedance of superconducting magnets by incorporating all relevant dynamic, electro-magnetic effects, such as persistent currents, inter-filament and inter-strand coupling currents and eddy currents in the strands and in the metallic components of the magnet. The aim is to establish a validated model that accurately represents the magnet's transient behavior. This model will be used as a reference for the simulation of anomalies, identifying any deviations in impedance from the nominal behavior.

The validation is performed against Transfer Function Measurements (TFM) of the MBRD. This magnet, part of CERN's High Luminosity LHC upgrade (HL-LHC), was recently tested in the CERN superconducting magnet test facility across a wide range of conditions. Additionally, artificial shorts were introduced by externally connecting resistances to some voltage taps across the magnet's coil turns, to imitate inter-turn shorts. The validation of the model with the experimental data, both with and without simulated shorts, provides deeper insight into how the complex impedance is affected by inter-turn shorts, offers references for a variety of scenarios, and supports the early detection of failures.

II. The MBRD Magnet and Measurement Set-Up

The MBRD magnet, developed by the Genova Laboratory of the National Institute for Nuclear Physics (INFN) in collaboration with CERN, plays a critical role in the HL-LHC upgrade by replacing the actual recombination dipole near the collision region [8].

Received 21 September 2024; revised 5 December 2024; accepted 12 December 2024. Date of publication 19 December 2024; date of current version 3 January 2025. This work was supported by the Wolfgang Gentner Programme of the German Federal Ministry of Education and Research under Grant 13E18CHA. *(Corresponding author: V. Reynaud.)*

V. Reynaud is with CERN, 1211 Geneve, Switzerland, and also with the Politecnico di Torino, 10129 Torino, Italy (e-mail: valentina.reynaud@cern.ch).

S. Farinon is with INFN, 16146 Genova, Italy.

M. Janitschke is with CERN, 1211 Geneve, Switzerland, and also with the University of Rostock, 18051 Rostock, Germany.

E. Ravaioli, A.P. Verweij, and G. Willering are with CERN, 1211 Geneve, Switzerland.

U. van Rienen is with the University of Rostock, 18051 Rostock, Germany.

Color versions of one or more figures in this article are available at https://doi.org/10.1109/TASC.2024.3520079.

Digital Object Identifier 10.1109/TASC.2024.3520079

TABLE I
ASSUMED MAIN CONDUCTOR PARAMETERS OF THE MBRD [10][11], [12]

Parameter	Unit	Value
Number of strands per turn	-	36
Bare cable width	mm	15.1
Bare cable height	mm	1.476
Strand outer diameter	mm	0.825
Strand twist pitch	mm	120
Cross-contact resistance	$\mu\Omega$	50
Filament twist pitch	mm	15
Filament diameter	μm	6
Copper-NbTi ratio	-	1.95
RRR of copper matrix	-	200

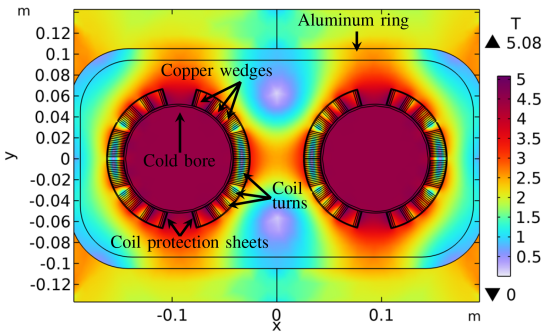

Fig. 1. Field map of the MBRD magnet simulated with COMSOL Multiphysics, showing the cold bore, the wedges, the coil protection sheets and the magnet coils. The model has been created using STEAM-pySIGMA [15], [16].

TABLE II
ASSUMED MAIN PARAMETERS OF THE MBRD MAGNET COMPONENTS [11], [13], [14]

Component	Volume [m^3]	Material	Assumed ρ [Ωm]
Al ring	$93.1 \cdot 10^{-3}$	Al alloy 6061-T6	$1 \cdot 10^{-12}$
CPS	$2.6 \cdot 10^{-3}$	Stainless steel	$600 \cdot 10^{-9}$
Cold bores	$8.5 \cdot 10^{-3}$	Stainless steel	$680 \cdot 10^{-9}$
Cu wedges	$25.4 \cdot 10^{-3}$	OF Copper	$1.11 \cdot 10^{-10}$

The MBRD is a 7.78 m long dipole magnet consisting of two asymmetrical apertures, with four coils comprising 31 turns each. They are wound with a Nb-Ti superconducting Rutherford cable, identical to the one used in the outer layer of the LHC's main dipole [9]. Assumed parameters of this cable are displayed in Table I.

Both apertures have a diameter of 105 mm and a beam separation of 188 mm [10]. The MBRD operates at 1.9 K with a nominal current of 12.34 kA, a nominal field in the center of the apertures of 4.5 T, and a corresponding nominal inductance of 30.5 mH. At low current, the inductance is 37.2 mH.

Fig. 1 shows the magnetic field over the cross-section of the magnet, comprising several metallic components. These components include the copper wedges that separate the coil blocks, the cold bore that insulates the coils from the beam region, the aluminum ring that maintains structural integrity by counteracting the electromagnetic repulsive forces between the two apertures, and the coil protection sheets (CPS) that protect the coils during the collaring process. The main parameters of these components are given in Table II.

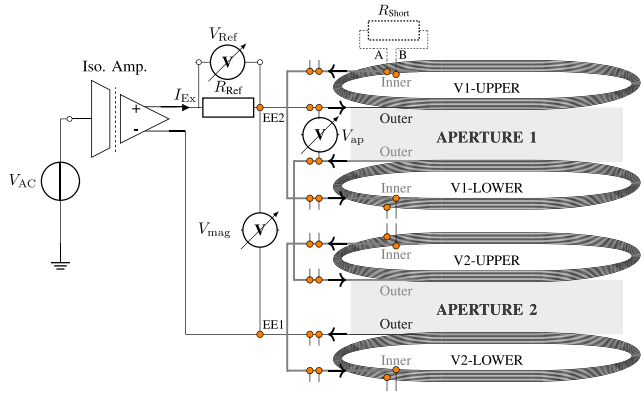

Fig. 2. Measurement system for the MBRD full magnet, showing a representation of the voltage taps (orange circles) used to measure the voltage across different turns. A short resistance is also included to illustrate how short-circuits can be imitated.

The setup used for measuring the complex impedance of the MBRD is depicted in Fig. 2. An AC voltage source, V_{AC} [V], with a peak amplitude of 10 V, generates a sinusoidal excitation current, I_{Ex} [A]. The insulation amplifier minimizes the effect of noise and electrically isolates the circuit from ground, directing the entire current into the magnet circuit. The gain-phase analyzer across the reference resistor, $R_{\mathrm{Ref}} = 25\,\Omega$, extracts both the real and imaginary components of the voltage $\boldsymbol{V}_{\mathrm{Ref}}$ [V]. The current is induced into the outer turn located at the midplane of the upper coil in the first aperture and is collected by the outer turn of the lower coil in the second aperture. It flows through the turns of each coil, following the path shown in Fig. 2.

Voltages can be measured using several voltage taps (depicted as orange circles). It can be measured across the entire magnet using voltage taps EE1 and EE2, across individual turns within the same coil (for example, using voltage taps A and B), or across different coils. The measured voltage $\boldsymbol{V}_{\mathrm{mag}}$ [V] is then used to calculate the complex impedance of the magnet as:

$$\boldsymbol{Z}_{\mathrm{mag}} = \frac{\boldsymbol{V}_{\mathrm{mag}}}{\boldsymbol{V}_{\mathrm{Ref}}} \cdot R_{\mathrm{Ref}}\ [\Omega] \tag{1}$$

A similar formula can be applied to calculate the impedance of a single aperture by replacing $\boldsymbol{V}_{\mathrm{mag}}$ with $\boldsymbol{V}_{\mathrm{ap}}$ [V], the voltage measured across that aperture.

Furthermore, external resistors can be connected to the voltage taps to imitate short circuits across different turns, as shown in Fig. 2, where voltage taps A and B are connected to the two pole turns of the upper coil in the first aperture.

III. MODELLING APPROACH

In network models, superconducting magnets can be represented by inductances L_{mag} [H], resistances R_{mag} [Ω], and stray capacitances to ground C_{gnd} [F]. The resistance drops to zero when the magnet is in superconducting state.

The behavior of superconducting magnets is subjected to a number of non-linear coupling effects, which consequently affect their impedance. In the physics-driven network model [6], each coupling phenomenon is represented by a coupling loop, consisting of an inductance L_{ec} [H], a resistance R_{ec} [Ω], and

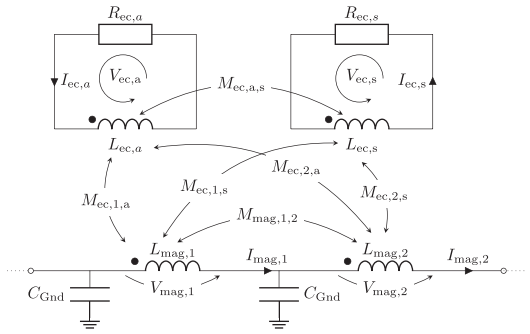

Fig. 3. Lumped element network model representing two equivalent loops coupled to two turns of a magnet [6].

a specific equivalent current I_{ec} [A]. The loops are coupled to each inductance in the magnets' circuit and interact with one another through mutual inductances, such as $M_{ec,1,a}$ [H] and $M_{ec,1,s}$ [H], as shown in the simplified schematic in Fig. 3. This approach incorporates effects such as inter-filament and inter-strand coupling currents [17][18], eddy currents in the strands, and eddy currents in the metallic components [6].

The lumped-element values for the eddy current loops are determined from the induced power loss, an equivalent induced current, and time constant. This is achieved through either analytical equations for conductor losses or COMSOL Multiphysics simulations for eddy currents in the metallic components, as their complex geometries make accurate assessment through analytical formulas unfeasible.

The complex current distribution within the laminated aluminum rings could not be accurately captured with the two-dimensional model. A scaling factor was therefore applied to the resistivity value in Table II in order to achieve a better agreement with the experimental measurements.

IV. Validation of the Model

The validation process for the MBRD is based on a comparison between the simulation results and measurements taken at 1.9 K without the presence of short circuits. Subsequently, the validation was extended to measurements with the external artificial shorts.

A. Validation of Simulations Without Artificial Short Circuits

The simulated impedance at 1.9 K without shorts, as shown in Fig. 4, shows good agreement for both the full magnet and single-aperture configurations. Only one aperture is shown for clarity, as the measured impedance in both apertures is nearly identical, with a maximum relative error of 0.9% up to 10 kHz. Simulations show that conductor losses, including coupling currents and magnetization effects, have a small effect on the impedance curve. Although these losses cause a slight deviation from the impedance curve of the ideal LC circuit, their impact is minor compared to the influence of eddy currents in the metallic components.

The maximum relative error between the measured and simulated impedance modulus remains below 12% up to 10 kHz, with an average error of 7.89% for the full magnet and 3.39% for one aperture. Beyond 10 kHz, the discrepancy in the results

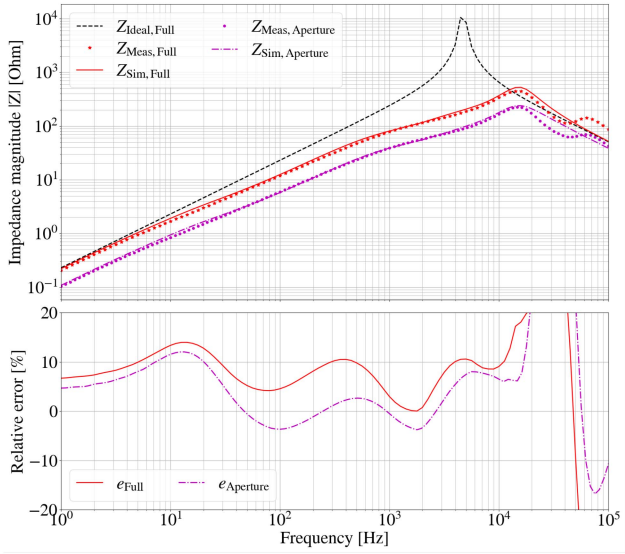

Fig. 4. Simulation and measurements of the MBRD impedance modulus of one aperture and the full magnet, and their relative error. For reference, the ideal LC circuit (L = 37.2 mH, C = 250 nF) is also shown.

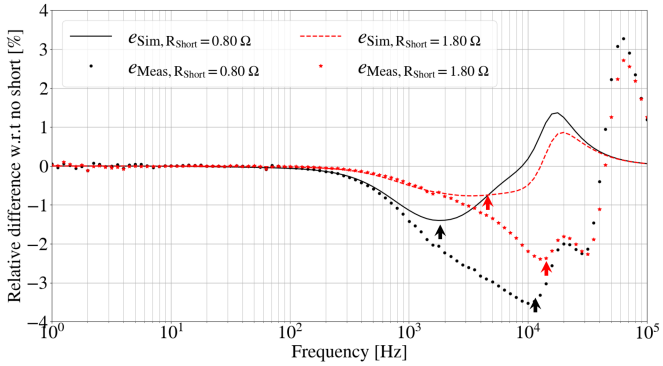

Fig. 5. Relative difference in the impedance magnitude between the case with and without short circuits for measurements and simulations. The specified short resistances have been connected across the voltage taps of the two pole turns.

exceeds 20%, most likely due to the simplification of the model in terms of lumping capacitances. For simplification, only three capacitances were included in the model, at the beginning, middle, and end of the magnet model.

B. Validation of Simulations With Artificial Short Circuits

In additional impedance measurements, two artificial short circuits with resistances of 0.8 Ω and 1.8 Ω were introduced across voltage taps A and B in the magnet.

Fig. 5 shows the measured and simulated relative difference in impedance magnitude, induced by the presence of these short resistances. While the simulated impedance changes do not precisely align with the measured changes, the overall relative difference agrees well up to 1 kHz, after which it diverges. Additionally, both the measured and simulated results demonstrate that increasing the short-circuit resistance value reduces the magnitude of the peak error, marked by the arrows in Fig. 5, while also shifting it to higher frequencies.

The discrepancies in peak magnitude likely arise from the difficulty in modeling the individual field contributions of each

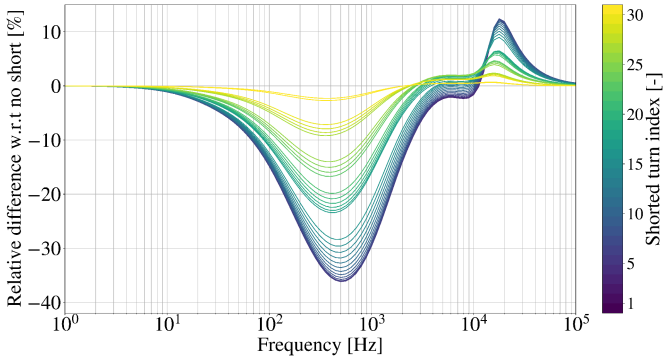

Fig. 6. Relative difference in the impedance magnitude between simulations without and with a short circuit resistance $R_S = 0.01\ \Omega$ across a single turn. The numbering of the turns refers to counter-clockwise rotation (Turn 1 at the midplane and Turn 31 at the pole).

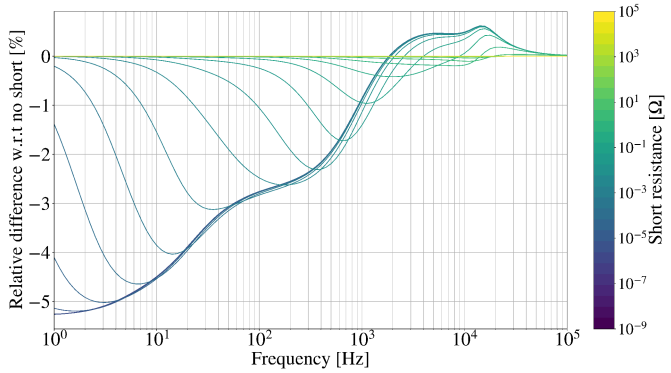

Fig. 7. Relative difference in the impedance magnitude between simulations without and with a short circuit resistance of various sizes across the pole turn.

turn and the complex capacitance distribution. Further work will concentrate on enhancing the simulations by accurately modeling the capacitance for each turn and improving the field mapping, as the current models do not account for the distinct contributions of each turn.

V. Effect of Short-Circuits

The effects of short circuits on the impedance are analyzed for different locations and varying resistance values. The impact of connecting a short-resistance $R_{\mathrm{Short}} = 0.01\ \Omega$ across different turns of the magnet, is shown in Fig. 6.

The analysis was conducted on the first coil of the first aperture of the magnet, which was modeled as 31 distinct subcircuits in the network. These short-circuits could therefore be simulated individually across each turn. The figure depicts the simulated relative difference between a reference simulation without short-circuit resistances and one with, revealing a significant impedance change, particularly in the frequency range up to 10 kHz. Although the model with short circuits was validated against measurements up to 1 kHz, the relative difference between simulations with and without shorts can still provide valuable insights across the entire frequency range.

As can be seen in the upper right section of the left aperture in Fig. 1, the turns situated in close proximity to the midplane are considerably more densely packed than those located at the pole. This leads to a larger mutual coupling between the turns in this region, and hence a larger change from the reference impedance in case of a short circuit across these turns. At higher frequencies, a shift in the resonance peak is observed as a consequence of the changed LC characteristic. The impedance difference ranges from 35% for turns near the mid-plane to a few percent for turns near the pole and a clear separation can be observed between the curves, depending on the spatial arrangement of the coils. This allows for distinct identification of the different coil blocks within the magnet.

Simulating short circuits with different resistance values enables a more detailed analysis of their impact on impedance. Fig. 7 presents the case where resistance values ranging from 1 nΩ to 100 kΩ are connected across the pole turn. At low frequencies, the short-circuit resistance is usually higher than the turn impedance, so most current flows through the inductance path. As the frequency increases, the current gradually shifts to the resistance branch until it flows entirely through the resistance. In the case of very low resistance values, the resistance is constantly less than the turn impedance, causing a change in the magnet impedance also at very low frequencies. As shown in Fig. 7, the relative difference from simulations without shorts across the pole turn ranges from 5% to less than 1%, with the largest differences occurring at higher frequencies for larger resistance values. Notably, the difference decreases to below 0.9% for a resistance value of 0.1 Ω.

VI. Conclusion and Outlook

The two-dimensional lumped element model was validated against impedance measurements of the HL-LHC recombination dipole. Additional measurements, incorporating short-circuit resistances across the voltage taps, were used to further validate the model.

Simulations for the MBRD showed that a short circuit becomes detectable when its resistance falls below a specific value, depending on the turns' location within the magnet. For reliable short-circuit detection, the relative difference between simulations with and without short circuits must exceed the relative difference observed between measurements in the two apertures by a value ranging from 1% to a few percent.

The simulations reveal that short circuits can be identified when the short resistance decreases below 50 Ω for mid-plane turns and 0.1 Ω for turns close to the pole. The variation of this value can be attributed to the decreasing mutual coupling between turns, by moving from the mid-plane to the pole.

In conclusion, the model accurately represents the complex impedance of superconducting magnets by including factors such as coupling losses, eddy currents in metallic components, and the effects of short circuits. Its capability to simulate transient behavior and provide insights into the impact of short resistance and their location demonstrates its significance for fault diagnosis.

ACKNOWLEDGMENT

The authors would like to thank A. Foussat and the CERN SM18 team for their help in the measurements, in particular, R. Bouvier and G. Ninet.

REFERENCES

[1] M. Janitschke, E. Ravaioli, A. Verweij, G. Willering, and U. van Rienen, "Complex impedance of the LHC main dipole magnet in the presence of artificial short circuits," *SUST*, 2024.

[2] H. Ehmler et al., "Comparative analysis of impulse and impedance tests to detect short circuits within the W7-X magnets," *IEEE Trans. Appl. Supercond.*, vol. 16, no. 2, pp. 767–770, Jun. 2006.

[3] K. Rieße, T. Rummel, G. Ehrke, and M. Koppen, "Design, tests, and repair procedures for the electrical insulation of the superconducting W7-X magnets," *IEEE Trans. Appl. Supercond.*, vol. 20, no. 3, pp. 447–450, Jun. 2010.

[4] H. Ehmler, I. R. Dixon, T. A. Painter, and J. A. Powell, "Electrical AC tests on CICC coil for series-connected hybrid magnet," *IEEE Trans. Appl. Supercond.*, vol. 22, no. 3, Jun. 2012, Art. no. 9002204.

[5] A. Foussat, L. Grand-Clement, D. Smekens, F. O. Pincot, L. Bortot, and F. Savary, "Frequency-domain diagnosis methods for quality assessment of Nb_3Sn coil insulation systems and impedance measurement," *IEEE Trans. Appl. Supercond.*, vol. 28, no. 3, Apr. 2018, Art. no. 4003505.

[6] M. Janitschke, M. Bednarek, E. Ravaioli, A. P. Verweij, G. Willering, and U. Van Rienen, "Physics-driven lumped-element modelling for impedance simulations of superconducting accelerator magnets," *Supercond. Sci. Technol.*, vol. 38, no. 1, Dec. 2024, Art. no. 015013, doi: 10.1088/1361-6668/ad9ad8.

[7] R. E. Shafer, "Eddy currents, dispersion relations, and transient effects in superconducting magnets," FERMILAB, Batavia, IL, Tech. Rep. FERMILAB-TM-991, Sep. 1980. [Online]. Available: http://cds.cern.ch/record/192894

[8] S. Farinon, P. Fabbricatore, S. Curreli, and E. Todesco, "The design of superconducting separation dipoles D2 for the high luminosity upgrade of LHC," *IEEE Trans. Appl. Supercond.*, vol. 26, no. 4, Jan. 2016, Art. no. 4001504.

[9] A. Bersani et al., "The superconducting separation dipoles MBRD for the high luminosity upgrade of LHC: From short model to prototype," *IEEE Trans. Appl. Supercond.*, vol. 29, no. 5, Aug. 2019, Art. no. 4003305.

[10] B. Caiffi et al., "The development of the superconducting dipoles D2 for the high luminosity upgrade of LHC," *IEEE Trans. Appl. Supercond.*, vol. 31, no. 5, Aug. 2021, Art. no. 4000405.

[11] O. Brüning et al., "LHC Design Rep," CERN, Geneva, Rep. CERN-2004-003-V-1, 2004. [Online]. Available: https://cds.cern.ch/record/782076

[12] Z. Charifoulline, "Residual resistivity ratio (RRR) measurements of LHC superconducting NbTi cable strands," *IEEE Trans. Appl. Supercond.*, vol. 16, no. 2, pp. 1188–1191, Jun. 2006.

[13] N. I. of Nuclear Physics in Genova (INFN), "Detail design of the aluminum sleeves for MBRD," CERN, Tech. Rep. MBRDP_DRW_00104_REV3, 2019. [Online]. Available: https://edms.cern.ch/ui/file/2137027/AC/lhcmbrdp0004-vAC.pdf

[14] N. I. of Nuclear Physics in Genova, "Design report of one aperture of the MBRD magnet," CERN, Tech. Rep. MBRDP1_00003, 2019. [Online]. Available: https://edms.cern.ch/ui/file/2137021/0/lhcmbrdc0002-v0.pdf

[15] "STEAM-PySIGMA website," Accessed: Jul. 20, 2024. [Online]. Available: https://steam.docs.cern.ch/tools/sigma/

[16] M. Maciejewski, C. Barbagallo, and B. Bokhraie, STEAM-sigma. In Workshop Slides., Jun., 2019, [Online]. Available: https://pypi.org/project/steam-pysigma/

[17] A. P. Verweij, "Electrodynamics of superconducting cables in accelerator magnets," Ph.D. dissertation, Twente U., Twente, 1995, presented on Sep. 15, 1995. [Online]. Available: https://cds.cern.ch/record/292595

[18] E. Ravaioli, B. Auchmann, M. Maciejewski, H. ten Kate, and A. Verweij, "Lumped-element dynamic electro-thermal model of a superconducting magnet," *Cryogenics*, vol. 80, pp. 346–356, 2016, [Online]. Available: https://www.sciencedirect.com/science/article/pii/S0011227516300832